



HAL
open science

Hierarchical mesoporous silica templated by the combination of fine emulsion and micelles

Violeta Claudia, Marie-José Stébé, Mélanie Emo, Bénédicte Lebeau, Jean-Luc Blin

► **To cite this version:**

Violeta Claudia, Marie-José Stébé, Mélanie Emo, Bénédicte Lebeau, Jean-Luc Blin. Hierarchical mesoporous silica templated by the combination of fine emulsion and micelles. *Microporous and Mesoporous Materials*, 2020, 305, pp.110376. 10.1016/j.micromeso.2020.110376 . hal-03060045

HAL Id: hal-03060045

<https://hal.science/hal-03060045>

Submitted on 13 Dec 2020

HAL is a multi-disciplinary open access archive for the deposit and dissemination of scientific research documents, whether they are published or not. The documents may come from teaching and research institutions in France or abroad, or from public or private research centers.

L'archive ouverte pluridisciplinaire **HAL**, est destinée au dépôt et à la diffusion de documents scientifiques de niveau recherche, publiés ou non, émanant des établissements d'enseignement et de recherche français ou étrangers, des laboratoires publics ou privés.

Hierarchical mesoporous silica templated by the combination of fine emulsion and micelles

Claudia Violeta Cervantes-Martinez¹, Marie-José Stébé¹, Mélanie Emo¹, Bénédicte Lebeau^{2,3},

Jean-Luc Blin^{1,*}

¹ Institut Jean Barriol, UMR CNRS 7053 L2CM, Université de Lorraine, Faculté des Sciences et Technologies, BP 70239, 54506 Vandoeuvre lès Nancy cedex, FRANCE

² : Université de Haute Alsace (UHA), CNRS, IS2M UMR 7361, F-68100 Mulhouse, France

³ : Université de Strasbourg, 67000 Strasbourg, France

*Corresponding authors

Pr. Jean-Luc Blin

Université de Lorraine

UMR CNRS 7053 L2CM

Faculté des Sciences et Technologies

BP 70239

F-54506 Vandoeuvre-lès-Nancy cedex, France

Tel. +33 3 83 68 43 70

E-mail: Jean-Luc.Blin@univ-lorraine.fr

ABSTRACT

Concentrated emulsions have been widely considered as templates for the preparation of macroporous structures. Replacing concentrated emulsions by fine ones should rather lead to materials having large mesopores. However, fine emulsions were barely investigated for this purpose. On the other hand, mesostructured silica SBA-15 can be prepared from Pluronic P123 micelles according to the cooperative templating mechanism. Starting from mixture of fine emulsion and Pluronic P123 micelles, it is expected to obtain silicas with a controlled hierarchical mesoporosity.

The fine emulsion has been formulated from the Kolliphor/Myristate/Water system. To get informations concerning the degree of compatibility between the two surfactants, which can affect the formation of the porous materials, the Kolliphor/P123/water system has been investigated in detail. The structural parameters of the mixed liquid crystal phases have been determined and the mixed micellar structure has been investigated by SAXS.

The hierarchical porous silicas have been synthesized combining fine emulsion and Pluronic micellar solution. The materials porosity features strongly depend on the weight proportion between the fine emulsion and the P123 micelles. If this proportion is lower than 5/5, mesoporous silicas present a dual mesoporosity. By contrast, by increasing this proportion the mesopore size distribution only shows large mesopores.

KEYWORDS: Fine emulsion; Mixed-system; Micellar structure; Biocompatible Surfactants; Silica materials; Hierarchical porosity

1. Introduction

Hierarchical porous materials, presenting interconnected pore at multiple length scales [1] such as micro-mesoporosity, meso-macroporosity or meso-mesoporosity, have applications in various domains such as photonics, bioengineering and nanotechnology [2-5]. Their importance comes from their properties such as a large surface area (around 1000 m²/g for silica), their large pore volume, and the presence of pores allowing the control of the diffusion [6,7]. For example, micro-macro or meso-macroporous materials are particularly interesting and useful in catalysis and drug delivery systems. From an application viewpoint, drugs or catalysts can be loaded in the mesopores and the micropores, while the macropores enhance the mass transfer and reduce the transport limitations [8,9]. This is particularly beneficial in the case of large molecules or in viscous systems where diffusion rates are low. The development of hierarchical porous materials at multiple scales was thus the subject of interest over the last few years. Different strategies have been developed to design these compounds [10-16]. One of them consists in combining the sol-gel chemistry and the use of surfactant molecules assemblies as framework templates. For example, Morris et al. employed mixtures of micellar solutions of nonionic surfactants, including Pluronic, Brij and Tetronic types, as templates for synthesizing porous silica materials having several pore sizes [17]. Depending on the surfactant mixture, ordered uniform pore size arrangements, partially ordered complex bimodal structures or totally disordered non-mesoporous structures were obtained.

The chemically induced liquid-liquid phase separation [18] has also been applied to synthesize mesoporous silica material with interconnected macropores. This technique is based on the hydrolysis and condensation of inorganic precursors in the aqueous domain, derived from the self-assembly phase of the used template. The earlier the phase separation takes place in the sol-gel transition, the larger the characteristic size of pores and gel skeletons

become. A wide variety of water soluble block copolymers, such as polyoxyethylene surfactants [1,10,19-23] has been used to control the phase separation/gelation kinetics in the preparation of monolithic silica exhibiting both interconnected macropores and templated mesopores. With the use of various silica precursors such as tetramethoxysilane, tetraethoxysilane and bis(trimethoxysilyl)-ethane, amorphous phase or mesopores with a disordered arrangement can be integrated in gel networks which constitute a co-continuous macroporous structure [11,19]. Using this approach, Nakanishi et al. synthesized monolithic silica gels with a hierarchical meso-macroporous structure via a spontaneous sol-gel process and yielded materials with highly ordered hexagonal arrays of mesopores [24]. The authors explain that the monolithic body with well-defined interconnected macropores is a result of concurrent phase separation and sol-gel transition induced by the polymerization reaction, whereas the mesopores are templated by the cooperative self-assembly of inorganic species and the assembly directing agent polyethylene oxide-block-poly-polypropylene oxide-block-polyethylene oxide. A versatile method widely used to get the macro-mesoporous materials consists in combining the emulsion templating method and the surfactant assembly templating one [25-30]. In that case the main role of oil is to act as a template for the generation of the macropore network. For example, using concentrated emulsions and micellar templates, Carn and co-workers [31] prepared hierarchical inorganic porous monoliths. These materials show interconnected macroporosity with disordered structures. The mesopore size varies from 1.2 to 4.0 nm. Tiddy and co-workers [10,32] also use this approach to achieve the room-temperature synthesis of a macro-mesoporous silica material during the natural creaming of oil-in-water emulsion. This synthesis was carried out using cetyltrimethylammonium bromide as surfactant and trimethylbenzene as oil. The obtained material has a high surface area (800 m²/g) with a narrow pore size distribution centered at around 4.0 nm. Monolithic silica foams bearing a cubic organization of the mesopores, obtained under alkaline condition with non-

ionic surfactant have been proposed by Esquena et al. [15,16]. Hierarchically macro-mesoporous monoliths using Pluronic P123 as porogen are also reported by different groups [1, 33-35]. Other imprints such as latex spheres [36] or solid lipid nanoparticles [37] can serve as mold to generate the macropores. If, as mentioned above, concentrated emulsions have been widely considered to design the macro-mesoporous materials, on the contrary, fine emulsions have been barely investigated to get large mesopores or dual mesoporous materials. Usually they are employed for practical applications, such as the preparation of polymeric nanoparticles, agrochemical applications, food technology, pharmaceutical and cosmetic fields [38-41]. We have recently reported that fine emulsions, stable for few days, can be formulated in the water rich part of the Kolliphor/Myristate/water system [42]. In this paper, in combination with the cooperative templating mechanism (CTM), we have used these fine emulsions as imprints to prepare dual mesoporous silicas. Before the synthesis of the materials, we have investigated in detail the Kolliphor/P123/water system to have informations concerning the possible interactions between the two surfactants, which can affect the formation of the porous materials.

2. Materials and methods

Kolliphor EL (denoted as KEL), a surfactant synthesized from the reaction of castor oil and ethylene oxide in a molar ratio 1:35 (BASF Corporation, technical literature), was purchased from Sigma Aldrich and used as received, without any further purification. The selected triblock copolymer is the Pluronic P123 (EO)₂₀(PO)₇₀(EO)₂₀, it was also purchased from Aldrich as well as the tetramethoxysilane (TMOS), used as the silica source and Myristate. Deionized water was obtained using a Milli-Q water purification system.

2.1. Phase diagram determination

Samples were prepared, by weighting the required amounts of surfactants and water in sealed glass tubes. The homogenization of the samples was induced by mixing with a vortex stirrer or by mechanical milling. To favor homogenization, the samples were also centrifuged several times at 3000 rpm during 5 to 10 minutes, depending on the surfactant amount. The Kolliphor/P123/water phase diagram has been established by preparing samples over the whole range of surfactants concentrations, keeping them in a water bath at 25 °C until reaching thermodynamic equilibrium (after few days). Observations with the eyes, combined with optical microscope equipped with cross polarizers (Olympus BX 50), were used to identify the different phases and to determine the phase boundaries. Small angle X-ray scattering measurements were additionally performed to establish the phase boundaries accurately, to confirm the nature of the different phases and to determine the space group of the cubic structures.

2.2. Silicas preparation

Preparation of the fine emulsion: Fine emulsion has been formulated from the Kolliphor/Myristate/water system using the Phase Inversion Composition (PIC) method, according to a procedure previously reported [42]. Here, the oil to surfactant ratio and the weight fraction of water have been fixed to 0.43 and 0.90, respectively. These conditions lead to formation of fine emulsion with a size, determined by DLS, of around 30 nm in diameter.

Preparation of the porous silica: First, a solution of fine emulsion (noted Em) at pH = 7 and a micellar solution of Pluronic P123 (5 wt.% at pH =0.3) in water are separately prepared. Then, both solutions are mixed in different proportions to get 10g of the final mixture. The fine emulsion/P123 micellar solution weight proportion (labelled as Em/P123) has been varied from 0/10 to 9/1. After that, tetramethoxysilane (TMOS) used as the silica source was

added. The quantity of silica, expressed as the P123/TMOS molar ratio, has been fixed to 0.005. The mixture was stirred at ambient temperature for 1 hour using a magnetic stirrer. Then, it was transferred and sealed in a Teflon autoclave. The autoclave was heated at 40°C for 24 h, afterwards at 100°C for 24 h. The final products were recovered after ethanol extraction with a Soxhlet apparatus for 48 h. After drying at room temperature during 24 h, samples were thermally treated under synthetic air as follow. A first temperature increase was applied at 2°C/min until 150°C with a 1 h plateau, followed by a second temperature ramp at 2°C/min to reach 350 °C. Temperature was held for 1 h, then, a final temperature ramp at 2°C/min was imposed to reach 550 °C with a 1 h plateau. The cooling process was uncontrolled and directed by the oven inertia.

2.3. Characterization

Small angle X-Ray scattering (SAXS) data were collected on a “SAXSess mc²” instrument (Anton Paar), using line-collimation system. This instrument is attached to a ID 3003 laboratory X-Ray generator (General Electric) equipped with a sealed X-Ray tube (PANalytical, $\lambda_{\text{Cu, K}\alpha} = 0.1542 \text{ nm}$) operating at 40 kV and 50 mA. Each sample was introduced in a “Special Glass” capillary for liquids and liquid crystals ($\Phi = 1.5 \text{ mm}$ and 2.0 mm for micellar solutions and liquid crystals, respectively), or between two sheets of Kapton® for materials, then placed inside an evacuated sample chamber at 23°C, and exposed to X-Ray beam. Scattering of X-Ray beam was registered by a CCD detector (Princeton Instruments, 2084 x 2084 pixels array with $24 \times 24 \mu\text{m}^2$ pixel size) at 309 mm distance from the sample. Using SAXSQuant software (Anton Paar), the 2D image was integrated into one-dimensional scattering intensities $I(q)$ as a function of the magnitude of the scattering vector $q = (4\pi/\lambda) \sin(\theta)$, where 2θ is the total scattering angle. Thanks to a translucent beamstop allowing the measurement of an attenuated primary beam at $q = 0$, all measured intensities

can therefore be calibrated by normalizing the attenuated primary intensity. Data were then corrected for the background scattering from the cell and for slit-smearing effects by a desmearing procedure from SAXSQuant software, using Lake method. For micellar solutions, after treatment, obtained intensities were scaled into absolute units using water as a reference material.

Nitrogen adsorption and desorption isotherms were determined on a Micromeritics TRISTAR 3000 sorptometer at - 196 °C over a wide relative pressure range from 0.01 to 0.995. The pore diameter and the pore size distribution were determined by the BJH (Barret, Joyner, Halenda) method [43] with KJS (Kruk, Jaroniec and Sayari) correction applied to both the adsorption and desorption branches of the isotherm. Although it is well known that this method gives an underestimated pore size and that some new methods have been developed, we use it here for the sake of simplicity and the use of this mathematical algorithm does not affect significantly our results as it is a systematic comparison.

The morphology of the samples was observed by Scanning Electron Microscopy (SEM), using a Philips FEI XL30 FEG microscope with an accelerating voltage = 7 kV. The samples were first metallised by a thin gold layer (< 10 nm).

The samples were also observed by transmission electron microscopy (TEM) using a JEOL ARM200-CFEG microscope operating at 200 kV. Samples in powder were first dispersed in chloroform with help of ultrasounds, and spread on gold observation grids covered by a formvar film.

3. RESULTS AND DISCUSSION

3.1. The Kolliphor/P123/water ternary diagram

The investigation of the Kolliphor/P123/water phase diagram shows that in the water rich part of the diagram (Fig. 1), at least up to a total surfactant concentration equal to 22 wt.%, a

micellar solution (L_1) is obtained, whatever the ratio between Kolliphor and P123. The L_1 domain is extended up to 46 wt.% of surfactant for solutions rich in Kolliphor. The cubic (I_1), the hexagonal (H_1) and the lamellar (L_α) liquid crystal domains appear as the total surfactant concentration increases. The limits of I_1 are unbroken and almost continuous between the pure cubic phase of Kolliphor and that of P123; i.e. from 46 to 58 wt. % of Kolliphor and from 22 to 37 wt.% of P123 (Fig. 1). In the same way, except for the Kolliphor-rich domain, which gives way to a reverse micellar phase, a hexagonal phase whose water quantity corresponds approximately to the one present in the pure liquid crystals of Kolliphor, and P123 appears. This observation suggests the existence of mixed liquid crystals [44,45]. For the pure Kolliphor system this phase is detected between 58 and 68 wt.% of Kolliphor in water, whereas it is located between 33 and 62 wt.% of Pluronic in the P123/water system. If the total surfactant concentration is further increased, the lamellar phase (L_α), which is not detected in the Kolliphor/water binary system appears. This mixed L_α phase can incorporate up to 71.5% of Kolliphor. For the richer part in Kolliphor, a reverse micellar phase (L_2) can be formed for total surfactant concentrations higher than 87%. This L_2 phase extends into a tongue shape when it is enriched in P123. Finally, a solid phase is observed for total surfactant concentrations higher than 97 wt.% if the P123 loading in the mixture is higher than 21%. Whatever the organized molecular system, the compatibility between the head groups, composed of oxyethylene units and of the alkyl chains of Kolliphor and P123, allows the formation of mixed entities in all proportion. No gap of miscibility is observed.

3.2 Micellar structure and determination of the structural parameters of the liquid crystals

To go further in the micelles characterization, SAXS experiments have been performed. Figure 2A presents the experimental SAXS spectra of mixed micellar solutions with a total

surfactant concentration of 5 wt.% in water for various ratios between Kolliphor and P123. The scattered intensity $I(q)$ is the product of the number of scattered particles by the structure factor and the form factor. All spectra present only one broad peak, characteristic of the form factor. It is shifted from 0.78 to 0.59 nm^{-1} when the quantity of P123 in the surfactants mixture varies from 0 to 100%. The presence of interactions highlighted at the lower q values is described by the structure factor. To determine the micellar structure, data were analyzed by using the Generalized Indirect Fourier Transform (GIFT) method [46,47], taking into consideration the interparticle interactions. The best fits (Fig. 2A solid line) have been obtained by considering the hard sphere model using the Percus-Yevick expression to take into account the structural factor [39-48]. The GIFT procedure shows that the form factor determined absolutely free from model assumptions correspond to sphere. From Figure 2A, it can be noticed that the data in low q deviate from fits. This is due to the fact that the hard sphere model, widely used, takes quite well into account the repulsive interactions, but it remains approximate. The considered parameters are the volume fraction of hard spheres, the radius of the globules and the polydispersity. Moreover, addition of an attractive potential could likely enhance the quality of the fit at the low q values. The obtained pair-distance distribution functions (PDDFs) are depicted in Figure 2B. The PDDF is calculated after obtaining the best matching between the experimental curve and the theoretical one, obtained by the GIFT method. All the curves present a bell-like shape, characteristic of spherical micelles, with a dimension which depends on the P123 content in the surfactants mixture. Its value progressively varies from 13.9 for the pure Kolliphor micelles to 24.3 nm for the pure P123 micelles (Table 1). It should be noted that the inhomogeneity of the micelles decreases with the P123 content. The inhomogeneity is characterized by a pronounced asymmetry in the $p(d)$ function on the left side of the second maximum. In the case of the Kolliphor micelles, the presence of a minimum with a negative value of $p(d)$ indicates that the globular structure

of the micelles is core-shell type because a difference in the core and shell scattering contrast exists [49]. The addition of P123 attenuates the contrast variation, since the PPO core and the PEO corona have similar electron densities. Similar behavior has been reported in literature [48,50]. For example, Schillén et al. [48] have shown that the increase of P123 content into $C_{12}(EO)_6$ micellar solutions decreases the inhomogeneity of the formed mixed micelles. In the study reported here, the $p(d)$ function presents a shoulder at around 3 nm for a Kolliphor/P123 ratio of 0.33 as for the P123 micelles, while a minimum is observed when this ratio is increased. The excess-electron density profiles have been determined by the deconvolution of the pair-distance distribution functions (PDDFs) (Fig. 2C). The profiles confirm the core-shell type particles for the different micellar solutions. Indeed, the negative density difference corresponds to the hydrophobic part, whereas the positive density difference can be attributed to the hydrophilic shell. The micelles diameter increases from 14.0 to 25.0 nm when the amount of P123 in the surfactants mixtures is changed from 0 to 100% (Table 1). These values are in accordance with the micelles sizes found by the GIFT analysis (Fig. 2B). When the Kolliphor/P123 ratio is decreased, more P123 molecules are accommodated in the micelles, leading to micelles with bigger size. The hydrophobic radius corresponds to the r -value when the sign of $\Delta\rho(r)$ changes. It can be estimated at 3.5 and 3.9 nm for the Kolliphor and P123 micelles, respectively. For the mixed systems, its value varies between 4.0 and 4.5 nm, depending on the P123 content (Table 1). The dimension of the alkyl chains in the micelles, corresponding to the lowest values of $\Delta\rho(r)$, can be estimated at about 2.5 and 3.8 nm respectively for the Kolliphor and P123 micelles. Given that, from the length of the bonds, the extended alkyl chains of Kolliphor have a dimension of about 2.5 nm, we can conclude that the alkyl chains, in the pure Kolliphor micelles, are rather extended. In the same way, estimating that the length of the PPO-part of the P123 is equal to 24.5 nm (1 PPO = 0.35 nm), we can deduce that the PPO chain, in the pure P123 micelles, can only be self-folded and

it rather adopts a meandering conformation as previously reported [35]. Looking at the dimension of the hydrophobic moieties in the mixed-micelles, around 3 nm, we can assume that the alkyl chains of Kolliphor and PPO chain of P123 likely adopt the same conformation than in the pure micelles.

All of the observations reported above support the existence of mixed micelles regardless the proportion between the two surfactants in the solutions.

Assuming that the mixture of the two surfactant forms a mixed entity, the structural parameters of the liquid crystal phases have also been determined. The water amount has been kept constant and the weight fraction of Kolliphor in the surfactant mixture, noted x_{KEL} , has been varied from 0 to 1. Figures 3, 4 and 5 show the SAXS spectra of the samples of the liquid crystal domain for a 40 wt.% of the Kolliphore-P123 mixture in water. The determination of the structural parameters is based on geometrical considerations and only the position of the reflection is taken into account. As for the micelles, the scattered intensity $I(q)$ is the product of the structure factor, which gives the position of the reflections, and the form factor, which depends on the electronic density of the different layers constituting the liquid crystal. So, for a given reflection, if the intensity of the form factor is weak, the resulting intensity of this reflection will also be weak. In addition, related to the structure factor the intensity of the reflections is attenuated with the order of the reflection. The combination of these two phenomena can thus intrinsically lead to reflection having weak intensities as observed on Figures 3, 4 and 5.

For a given composition the average molar weight (M) of the mixed entity is

$$M = \frac{n^P M^P + n^{KEL} M^{KEL}}{n^P + n^{KEL}}$$

where n^P and n^{KEL} respectively stand for the mole number of Pluronic and Kolliphor surfactant; M^P and M^{KEL} are the corresponding molar weight.

Cubic liquid crystal phase: For the cubic phase, the hydrophobic radius R_H is related to the lattice parameter a by the following equation [51] :

$$\frac{V_B}{V_S + \alpha V_W} = \frac{4 \nu \pi R_H^3}{3a^3}$$

with ν the number of micelles per cubic lattice. α stands for the number of water molecules per surfactant molecule and V_s, V_B, V_w respectively correspond to the molar volumes of the mixed surfactant, the hydrophobic part of the mixed surfactant and water ($V_w = 18 \text{ cm}^3/\text{mol}$). V_s and V_B depend on the molar ratio between the two amphiphiles. For example, for a mixture containing 30 wt.% of Kolliphor, these values are $V_s = 4016 \text{ cm}^3/\text{mol}$ and $V_B = 2656 \text{ cm}^3/\text{mol}$. The values of V_s and V_B for the pure surfactant were calculated from densities and are $V_s = 2354 \text{ cm}^3/\text{mol}$, $V_B = 834 \text{ cm}^3/\text{mol}$ for Kolliphor and $V_s = 5577 \text{ cm}^3/\text{mol}$ and $V_B = 4030 \text{ cm}^3/\text{mol}$ for P123.

Then, the cross sectional area S can be deduced as [51]:

$$S = \frac{3 V_B}{N R_H}$$

N is the number of Avogadro.

Scattering spectra of samples belonging to the cubic domain are reported in Figure 3A. Until

$x_{\text{KEL}} = 0.8$, the relative positions of the Bragg reflections are , $\sqrt{\frac{4}{3}}$, $\sqrt{\frac{8}{3}}$, $\sqrt{\frac{11}{3}}$, $\sqrt{\frac{12}{3}}$, $\sqrt{\frac{16}{3}}$

and $\sqrt{\frac{20}{3}}$. According to results published by Tiddy et al. [52], they can be indexed in the

Fm3m space group ($\nu = 4$). The cell parameter a is related to the d- spacing by the relations :

$$a = d_{111} \sqrt{3} .$$

Hexagonal liquid crystal phase: The hexagonal phase is composed of infinite cylinders packed in a hexagonal array. In case of direct systems, cylinders are filled by the hydrophobic chains and are covered by both head groups and water. The hexagonal phase is characterized

by its typical SAXS profile with the relative peak positions, 1, $\sqrt{3}$, 2 (Fig 4A). The distance d_{100} associated to the first peak is related to the hydrophobic core radius R_H by the relation [51]:

$$\frac{V_B}{V_S + \alpha V_W} = \frac{\sqrt{3}\pi R_H^2}{2d_{100}^2}$$

The cross-sectional area S can then be deduced from the following relation [51]:

$$S = \frac{2 V_B}{N R_H}$$

Lamellar liquid crystal phase: The lamellar phase can be described as an infinite bilayer of surfactants stacked in a parallel manner. The diffraction pattern exhibits two reflections with the relative peak positions 1, 2 (Fig. 5A). The repetition distance corresponds to the layer spacing, which comprises the water separated by the surfactant bi-layer. The cross-sectional area can be calculated from the following formula [51]:

$$S = \frac{2(V_S + \alpha V_W)}{N d_{001}}$$

where d_{001} stands for the repetition distance.

The hydrophobic thickness d_B and the hydrophilic thickness d_A can be deduced from the following equations [51] :

$$d_B = \frac{2V_B}{S} \text{ and } d_A = d_{001} - d_B$$

Figures 3B, 4B and 5B display the variation of structural parameters as a function of x_{KEL} for the cubic, the hexagonal and the lamellar liquid crystal phases, respectively. The dash lines are just a guide for the eyes, they do not correspond to fits. We can note from these figures that with the increase of x_{KEL} , whatever the liquid crystal, all the structural parameters vary in a linear manner as a function of the Kolliphor amount in the surfactants mixtures. As an example, for the cubic phase R_H and S decrease from 5.9 to 4.6 nm and from 2.3 to 1.3 nm² when x_{KEL} is changed from 0.30 to 0.80 (Fig. 3B). The linear relationship between the

structural parameters and the weight fraction of Kolliphor (x_{KEL}) in the surfactants mixtures is in a good agreement with the formation of a mixed liquid crystal phases in which both the Kolliphor and P123 molecules are present without segregation of the surfactants. The formation of mixed entities is possible thanks to the compatibility of the hydrophilic and the hydrophobic parts of the two surfactants.

Figure 3C, 4C and 5C describe the evolution of the structural parameters as a function of α , the number of water molecules per surfactant molecule. The dash lines are just a guide for the eyes, they do not correspond to fits. We can note an increase in the d-spacing due to the hydration of the head group and to the film formed between the layers of surfactants. As it could be expected for mixed liquid crystal phases, the variation of the structural parameters as a function of α follows the same trend than as a function of x_{KEL} . Indeed, in that case, even if the water content is constant, since the proportion between Kolliphor and P123 varies in the surfactant mixture, the average molar weight (M) of the mixed entity is changed for each content of Kolliphor present in the mixture. The number of surfactant molecules is thus modified and consequently, α which is the number of water molecules per surfactant molecules also varies when x_{KEL} is increased from 0 to 1.

It has been reported that in the pure P123 H_1 and I_1 domains, the values of R_H are around 4.8 and 4.5 nm, respectively [35,53]. Taking into account the different bonds, the length of the extended PPO block is 24.5 nm and comparing this value to the hydrophobic radius, it was concluded that the hydrophobic chains of the P123 hexagonal and cubic phases are completely self-folded. In the pure Kolliphor/water system, from the length of the bonds the dimension of the extended alkyl chains it was concluded that in H_1 and I_1 the alkyl chains adopt an extended conformation. Looking at the R_H values reported in Figure 3 and 4, we can therefore assume that, in the mixed hexagonal and cubic phases, the alkyl chains are also completely extended, whereas the PPO blocks are self-folded.

In the L_α phase, d_B varies from 7.8 to 3.8 nm when x_{KEL} is increased from 0 to 0.8 (Fig.5), considering the dimensions of the alkyl chains and of the PPO units in an extended conformation, the variation of d_B suggests that the hydrophobic parts in the mixed lamellar phase are rather extended.

3.3. Silica porous materials

Porous materials are prepared by combining the fine emulsion and the P123 micelles. From Figure 6, which presents the variation of the SAXS pattern as a function of Em/P123 weight proportion, it can be noted that under the synthetic conditions reported in this study, no mesopore ordering is recovered when P123 micelles are used alone as templates. Indeed, in that case no peak is detected on the SAXS pattern. For Em/P123 proportions comprised between 2/8 and 4/6, two peaks around 12 and 7 nm are observed on the SAXS patterns (Fig. 6). Their relative position $1, \sqrt{3}$ shows that in this range of Em/P123 proportions, ordered mesostructured silica materials are recovered. The unit cell a_0 , which is the sum of the pore diameter and of the thickness of the pore wall, can be deduced from the following relation: $a_0 = 2d_{100}/(3)^{1/2}$, and its value is found around to 13.9 nm. Increasing Em/P123 from 5/5 to 8/2, no secondary reflections are detected any longer. Only a broad peak characteristic of a wormhole-like mesostructure, as observed for MSU, is detected at 13.0 nm for Em/P123 = 5/5 (Fig. 6). This peak gives an indication of the average pore-to-pore distance in the disordered wormhole framework, which presents a lack of long-range crystallographic order. It is shifted towards smaller q values, when the Em/P123 proportion is raised until 8/2 (Fig. 6). Beyond Em/P123 = 8/2, no reflection is detected anymore on the SAXS pattern, meaning that the channel arrangement is completely random. The silica porous materials were observed by TEM (Fig. 7). For Em/P123 proportions of 0/10 and 1/9 materials are made of aggregated nanoparticles of about 5 nm in diameter and delimiting interparticle porosity. When Em/P123

proportion increases from 2/8 to 4/6, large mesopores regularly spaced and regular in size and shape are observed. Mesopores appear as spherical cavities of about 9-10 nm in diameter and delimited by continuous silica walls that indicate intraparticle porosity. The shape of these mesopores is consistent with the fact that mixed micelles serve as gabarit for mesopores and the silica network was formed around them. For the Em/P123 proportion of 2/8, well-ordered arrays of mesopores are observed. From Em/P123 of 5/5 to 8/2, large mesopores are still observed but they are less ordered and they appeared less regular in shape and size. Nevertheless, pore walls are still formed by a continuous silica network confirming the intraparticle porosity. When the Em/P123 proportion is up to 9/1, mesopores are barely observed to completely disappear in absence of P123. In absence of P123, the material is constituted of nanoparticles and does not exhibit anymore intraparticle porosity.

The sample prepared from the pure P123 micellar solutions exhibits a type IV isotherm (Fig. 8), characteristic of mesoporous materials according to the IUPAC classification [54]. The pore size distribution presents a maximum at around 3.8 nm (insert of fig. 8). The values of the specific surface area and of the pore volume are 818 m²/g and 0.52 cm³/g, respectively (Fig. 9). Preparing the silica materials from the P123 micelles and fine emulsion mixture, the isotherm remains type IV until a Em/P123 weight proportion of 5/5. It should be noted that with the addition of Em, the capillary condensation step is more pronounced and is shifted towards higher relative pressure, for example it occurs at $p/p_0 = 0.45$ for the material prepared from the pure P123 micelles, and at $p/p_0 = 0.75$ for the sample synthesized with a Em/P123 proportion higher from 1/9 to 5/5 (Fig. 8). Since the p/p_0 position of the inflection point is related to the pore diameter according to the Kelvin's equation, it can be inferred that bigger mesopores appear when the porous silicas are prepared from the Em/P123 mixture. Nevertheless, on the mesopore size distribution, the component at 3.7 nm is observed until a Em/P123 weight proportion of 4/6. A second maximum at 10.4 and 9.9 nm is observed for

materials prepared in the presence of 10 and 20% of Em, respectively. Thus, materials synthesized under these conditions present at least a dual mesoporosity. Increasing the Em/P123 from 2/8 to 5/5, the component at 3.8 nm disappears in favor of a doubling of the one at 10 nm, which is split into two maxima one around 10 nm and the other one at around 11 nm (Insert of Fig. 8). The intensity of the two peaks gradually reversed when the Em/P123 proportion is increased. Beyond Em/P123 = 5/5, the mesopore size distribution becomes broader and only one large component with a maximum between 16.5 and 24.3 nm (insert Fig.8). It should be noted that, whatever the Em/P123 proportion, both the mesopore size distribution and the shape of the isotherms at very low relative pressure suggest also the presence of micropores. It is interesting to look at the hysteresis shape at the desorption that is H2b type at low Em amount (from 2/8 to 5/5 weight proportions), then H1 type at higher Em amounts (from 6/4 to 8/2 weight proportions) [55]. The H2b hysteresis characterizes interconnected cage-like pores (cells), this is consistent with TEM observations that show only spherical pores regular in size but poorly spatially arranged except for 2/8 proportion. The H2b hysteresis is associated with a pore-blocking phenomenon with larger size distribution of pore neck sizes (cell windows) and has been observed for mesocellular silica foams. Pore size calculated from adsorption branch corresponds to the cell diameter and pore size calculated from desorption branch to the window size (Fig. S1). The H2b-H1 hysteresis sequence suggests mesocellular foam type materials with increasing pores neck size when Em amount increases and, in parallel, as supported by TEM and SAXS analyses, an increase of pore size with a loss of both the pore size regularity and the pore organization [56].

The specific surface area is quite high (Fig. 9) and it slightly increases when the proportion of Em is raised. For example, its value varies from 899 to 1003 m²/g when the Em/P123 proportion is changed from 1/9 to 8/2, respectively. Also, from Figure 8, you can see that the

pore volume gradually increases from 0.52 to 1.57 cm³/g as a function of the Em/P123 weight proportion.

Figure 10 shows SEM pictures of the samples synthesized at different Em/P123 weight proportions. The morphology of the materials can be mainly described as an agglomerate of small spheres having a diameter less than 10 μm. Higher the Em/P123 proportion is, more agglomerated the spheres are (Fig. 10). Besides the spheres, monolithic blocs with macropores of a few microns can also be detected, in particular for silica prepared with a Em/P123 proportion of 3/7 and 4/6.

3.4. Discussion

When pure P123 micelles are used as template, the mesostructured silicas are obtained through the Cooperative Templating Mechanism (CTM). In the initial step, when the silica is added to the micellar solution, hydrogen-bonding interactions between the oxygen atoms of the oxyethylene groups of the surfactant and OH groups of the hydrolyzed TMOS are formed. Then, the condensation of the inorganic precursor at the external surface of the micelles occurs. The mesophase is obtained after intermicellar condensation. Finally, the hydrothermal treatment at higher temperature completes the assembly of micelles and the polymerization of the silica source. The mesostructured material is recovered after surfactant removal by solvent extraction and/or by calcination. Under the conditions reported here, no mesopore ordering is obtained and the mesopore size distribution is centered at around 3.8 nm. Consequently, preparing the porous silica from the P123 micelles and fine emulsion mixtures, the component at 3.8 nm observed until a Em/P123 weight proportion of 3/7 can be attributed to mesopores templated by the pure P123 micelles.

To explain the evolution of the pore size distributions as a function of the Em/P123 proportion, we have also to consider the potential effect of methanol, released during the

hydrolysis on both the micellar solution and the fine emulsion. In previous studies we have shown that while the methanol does not significantly disturb the CTM mechanism for the preparation of mesostructured silica [57], it has a negative effect on the stability of the fine emulsion [58]. Indeed, in the case of nano-emulsions formulated from the Remcopal/decane/water system, we have reported that the methanol addition leads to an increase of the size of the oil droplets and to a destabilization of the nano-emulsion. Moreover, the existence of the nano-emulsions is not favored in the presence of the Pluronic micelles since the system becomes more hydrophilic [58]. Here, up to a Em/P123 proportion of 5/5, since P123 micelles predominate and since there is a huge amount of methanol released, from 17 to 10 wt. % (Fig. 10), we can assume that the negative effects of both methanol and P123 micelles involve a destabilization of the fine emulsion. The Kolliphor molecules arising from the destabilization of the fine emulsion likely associate with P123 to form mixed-micelles, which can eventually be swollen by Myristate. Indeed, the investigation of the Kolliphor/P123/water phase diagram has shown that the mixture of these two surfactants leads to the formation of mixed organized molecular systems and in particular mixed micelles. The formation of the mixed micelles is supported by the disappearance of the component at 3.8 nm in the mesopore size distribution when P123 micelles no longer predominate. This strongly suggests that the P123 micelles accommodate the Kolliphor molecules. The mixed micelles are likely responsible for the mesopore diameter at around 10 nm. Indeed, this value is in accordance with the hydrophobic size of these micelles (between 8.0 and 9.6 nm, depending on the Kolliphor/P123 proportion). Moreover, this is confirmed by TEM images that clearly show large spherical mesopores of about 9-10 nm in diameter. The swollen mixed micelles by Myristate give the peak at around 10.0 nm. As observed by the SEM the oil droplets arising from the fine emulsion can also coalesce to lead to the formation

of emulsion, which induces the presence of macropores having a size of few microns in diameter.

With the increase of the Em/P123 weight proportion beyond 5/5, the proportion of Pluronic micelles is lowered and less and less of methanol is released (Fig. 11). Indeed, it should be reminded that the TMOS amount has been fixed to get a P123/TMOS molar proportion of 0.005. Due to the lower amount of methanol and P123 micelles, the fine emulsion is not destabilized and we can assume that the porosity mainly arises from the fine emulsion, which proportion increases with the Em/P123 proportion. In that case, the hydrolyzed TMOS interacts with the Kolliphor molecules at the surface of the Myristate droplets, leading to the formation of silicas with large mesopores.

Finally, for all samples the microporosity can arise from the penetration of the oxyethylene units in the silica framework. After surfactant removal, this leads to the formation of micropores. This phenomenon is well reported in the literature for the synthesis of SBA-15 [59,60].

4. Conclusion

Among the different templates used to design porous materials, until now fine emulsions have been barely considered to prepare silicas with large mesopores. In this context, using a mixture of fine emulsion (Em) and Pluronic P123 micelles hierarchical porous silicas have been prepared. The porosity features of the materials strongly depend on the Em/P123 weight proportion. Indeed, if this proportion is lower than 5/5 dual mesoporous silica are obtained. In that case, methanol released during the hydrolysis of TMOS and the presence of P123 micelles have a negative effect on the fine emulsion, which is destabilized. The Kolliphor molecules likely associate with the P123 micelles to form mixed micelles. Indeed, the investigation of the Kolliphor/P123/water systems have shown that when both surfactants are

mixed, they formed mixed micelles and liquid crystal phases (cubic, hexagonal and lamellar). A part of Myristate released by the fine emulsion can swell the mixed micelles and the coalescence of the oil droplets can also give macropores. Increasing the Em/P123 weight proportion, both the proportion of P123 micelles and of methanol decrease and the fine emulsion is much more stable. The porosity is then controlled by the fine emulsion and silicas with large mesopores are obtained. Whatever the Em/P123 proportion micropores are also formed likely by the penetration of the EO groups in the silica framework.

Conflicts of interest

The authors declare that they have no competing interests

Acknowledgements

Claudia Violeta Cervantes-Martinez also thanks the CONACYT for the financial support of her PhD. Loïc Vidal in charge of the Electronic Microscopy platform of IS2M is warmful thanked for the TEM observations.

Funding:

This work was supported by the Consejo Nacional de Ciencia y Tecnología (Mexico) [grant number 243204/439621].

References

- [1] B.L. Su, C. Sanchez, X.Y. Yang, Hierarchically structured porous materials: from nanoscience to catalysis, separation, optics, energy, and life science, second ed., Wiley-VCH Verlag & Co. KGaA, Weinheim, Germany, 2012.
- [2] L. F. F. P. G. Braganca, M. Ojeda, J.L.G. Fierro, M.I. Pais da Silva, *Appl. Catal. A-Gen.* 423-424 (2012) 146.
- [3] P. Botella, A. Corma, M. Quesada, *J. Mater. Chem.* 22 (2012) 6394.
- [4] P. Perego, R. Millini, *Chem. Soc. Rev.* 42 (2013) 3956.
- [5] S.Y. Park, M. Barton, P. Pendleton, *Colloids and Surfaces A: Physicochem. Eng. Aspects* 385 (2011) 256.
- [6] F. Schüth, *Angew. Chem. Int. Ed.* 42 (2003) 3604.
- [7] B.T. Holland, C.F. Blanford, T. Do, A. Stein, *Chem. Mater.* 11 (1999) 795.
- [8] M.O. Coppens, G.F. Froment, *Fractals* 5 (1997) 493.
- [9] M.A. Parlett, K. Wilson, A.F. Lee, *Chem. Soc. Rev.* 42 (2013) 3876.
- [10] T. Sen, GJT. Tiddy, J.L. Casci, M.W Anderson, *Chem. Commun.* 17 (2003) 2182.
- [11] K. Nakanishi, Y. Kobayashi, T. Amatani, K. Hirato, T. Kodaira, *Chem. Mater.* 16 (2004) 3652.
- [12] J.L. Blin, B. Bleta, J. Ghanbaja, M.J. Stébé, *Microporous Mesoporous Mater.* 94 (2006) 74.
- [13] H. Mori, M. Uota, D. Fujikawa, T. Yoshimura, T. Kuwahara, G. Sakai, T. Kijima, *Microporous Mesoporous Mater.* 91 (2006) 172.
- [14] O. Sel, D. Kuang, M. Thommes, B. Smarsly, *Langmuir* 22 (2006) 2311.
- [15] J. Nestor, A. Vichez, C. Solans, J. Esquena, *Langmuir* 29 (2013) 432.
- [16] J. Esquena, J. Nestor, A. Vichez, K. Aramaki, C. Solans, *Langmuir* 28 (2012) 12334.

- [17] L. Chen, J. Xu, W.H. Zhang, J.D. Holmes, M.A. Morris, *J. Colloid and Interface Sci.* 353 (2011) 169.
- [18] K. Nakanishi, *J. Porous Mater.* 4 (1997) 67.
- [19] Y. Sato, K. Nakanishi, K. Hirao, H. Jinnai, M. Shibayama, Y.B. Melnichenko, G.D. Wignall, *Colloids Surfaces A Physicochem. Eng. Asp.* 187-188 (2001) 117.
- [20] X.Y. Yang, L.H. Chen, Y. Li, J.C. Rooke, C. Sanchez, B.L. Su, *Chem. Soc. Rev.* 46 (2017) 481.
- [21] G. Hasegawa, T. Yano, H. Akamatsu, K. Hayashi, K. Nakanishi, *J. Sol-Gel Sci. Technol.*, (2020) <https://doi.org/10.1007/s10971-020-05236-9>.
- [22] N. Huesing, C. Raab, V. Torma, A. Roig, H. Peterlik, *Chem. Mater* 15 (2003) 2690.
- [23] T. Amatani, K. Nakanishi, K. Hirao, T. Kodaira, *Chem. Mater.* 17 (2005) 2114.
- [24] K. Nakanishi, Y. Sato, Y. Ruyat, K. Hirao, *J. Sol-Gel Sci. Technol.* 26 (2003) 567.
- [25] A. Imhof, D.J. Pine, *Nature* 389 (1997) 948.
- [26] H. Zhang, G.C. Hardy, M.J. Rosseinsky, A.I. Copper, *Adv. Mater.* 15 (2003) 78.
- [27] B.P. Binks, *Adv. Mater.* 14 (2002) 1824.
- [28] C. Oh, S.C. Chung, S.I. Shin, Y.C. Kim, S.S. Im, S.G. Oh, *J. Colloids Interface Sci* 254 (2002) 79.
- [29] C. Zhao, E. Danish, N.R. Cameron, R. Katak, *J. Mater. Chem.* 17 (2007) 2446.
- [30] S. Zhang, J. Chen, *Polymer* 48 (2007) 3021.
- [31] F. Carn, A. Colin, M.F. Achard, H. Deleuze, E. Sellier, M. Birot, R. Backov, *J. Mater. Chem.* 14 (2004) 1370.
- [32] T. Sen, G.J.T. Tiddy, J.L. Casci, M.W. Anderson, *Microporous Mesoporous Mater.* 78 (2005) 255.
- [33] H. Zhong, G. Zhu, J. Yang, P. Wang, Q. Yang, *Microporous Mesoporous Mater.* (2007) 259.

- [34] A. Feinle, M. S. Elsaesser, N. Hüsing *hem. Soc. Rev.* 45 (2016) 3377.
- [35] A. Roucher, M. Emo, F. Vibert, M.J. Stébé, V. Schmitt, F. Jonas, R. Backov, J.L. Blin, *J. Colloid Interface Sci.* 533 (2019) 385.
- [367] B.T. Holland, C.F. Blanford, A. Stein, *Science* 281 (1998) 538.
- [37] R. Ravetti-Duran, J.L. Blin, M.J. Stébé, C. Castel, A. Pasc, *J. Mater. Chem.* 22 (2012) 21540.
- [38] L. Wang, X. Li, G. Zhang, J. Dong, J. Eastoe, *J. Colloid Interface Sci.* 314 (2007) 230.
- [39] N. Sadurní, C. Solans, N. Azemara, M.J. García-Celma, *Eur. J. Pharm. Sci.* 26 (2005) 438.
- [40] M. Jaworska, E. Sikora, M. Zielina, J. Ogonowski, *Acta Biochim. Pol.* 60 (2013) 779.
- [41] N. Anton, J.P. Benoit, P. Saulnier, *J. Controlled Release* 128 (2008) 185.
- [42] C.V. Cervantes-Martinez, M. Emo, M.J. García-Celma, M.J. Stébé, J.L. Blin, *Chem. Eng. Res. Des.* 151 (2019) 179.
- [43] E.P. Barrett, L.G. Joyner, P.P. Halenda, *J. Am. Chem. Soc.* 73 (1951) 373.
- [44] J.C. Ravey, A. Gherbi, M.J. Stébé, *Prog. Colloid Polym. Sci.* 79 (1989) 272.
- [45] K. Tamori, K. Esumi, K. Meguro, *J. Colloid Interface Sci.* 142 (1991) 236.
- [46] O. Glatter, O. Kratky, Academic Press, (1982) 167.
- [47] G. Fritz, O. Glatter, *J. Phys.: Condens. Matter* 18 (2006) S2403.
- [48] D. Löf, M. Tomšič, O. Glatter, G. Fritz-Popovski, K. Schillén, *J. Phys. Chem. B* 113 (2009) 5478.
- [49] B. Weyerich, J. Brunner-Popela, O. Glatter; *J. Appl. Cryst.* 32 (1999) 197.
- [50] M. Tomšič, M. Bešter-Rogač, A. Jamnik, W. Kunz, D. Touraud, A. Bergmann, O. Glatter, *J. Colloid Interface Sci.* 294 (2006) 194.
- [51] M. Alibrahim, M.J. Stébé, G. Dupont, J.C. Ravey, *J. Chim. Phys. Phys. - Chim. Biol.* 94 (1997) 1614.

- [52] P. Sakya, J.M. Seddon, R.H. Templer, R.J. Mirkin, G.J.T. Tiddy, *Langmuir* 13 (1997) 3706.
- [53] K. Assaker, I. Naboulsi, M.J. Stébé, M. Emo, J.L. Blin, *J. Colloid Interface Sci.* 446 (2015) 170.
- [54] K.S.W. Sing, D.H. Everett, R.A.W. Haul, L. Moscou, R.A. Pierotti, J. Rouquerol, T. Siemieniewska, IUPAC, *Pure and Appl. Chem.* 57 (1985) 603.
- [55] M. Thommes, K. Kaneko, A.V. Neimark, J.P. Olivier, F. Rodriguez-Reinoso, J. Rouquerol, K.S.W. Sing, *Pure Appl. Chem.* 87 (2015) 1051.
- [56] W.W. Lukens, P. Yang, G.D. Stucky, *Chem. Mater.* 13 (2001) 28.
- [57] K. Zimny, J.L. Blin, M.J. Stébé, *J. Colloid Interface Sci.* 330 (2009) 456.
- [58] P. Riachy, M.J. Stébé, B. Lebeau, A. Pasc, L. Vidal, J.L. Blin, *Microporous Mesoporous Mater.* 221 (2016) 228.
- [59] A. Galarneau, M. Nader, F. Guenneau, F. Di Renzo, A. Gedeon, *J. Phys. Chem. C* 111 (2007) 8268.
- [60] T. Benamor, L. Vidal, B. Lebeau, C. Marichal, *Microporous Mesoporous Mater.* 153 (2012) 100.

Figures caption

- Figure 1 : Composition phase diagram (wt.%) at 25°C of the Kolliphor/P123/water system. L_1 and L_2 represent the direct and reverse micellar phase, respectively. I_1 and H_1 denote respectively a direct micellar cubic phase and hexagonal phase. L_α is employed for the lamellar phase. S denotes a solid.
- Figure 2 : Experimental (dotted line) and approximated (GIFT) (solid line) SAXS spectra of mixed micellar solutions of Kolliphor and P123 with a total concentration of surfactant in water equal to 5 wt% at 25 °C. The Kolliphor/P123 proportions are indicated on the right (A); Corresponding pair-distance distribution functions (PDDFs) (B); Corresponding excess-electron density profiles (C).
- Figure 3 : Cubic liquid crystal phase : Evolution of the SAXS patterns of the cubic phase with the Kolliphor (KEL) content in the surfactants mixture (A) and structural parameters of I_1 as a function of x_{KEL} (B) and α (C); ■ : d_{111} , ○ : R_H and ▲: S. The total surfactant concentration is 40 wt.%.
- Figure 4 : Hexagonal liquid crystal phase : Evolution of the SAXS patterns of the hexagonal phase with the Kolliphor (KEL) content in the surfactants mixture (A) and structural parameters of H_1 as a function of x_{KEL} (B) and α (C); ■ : d_{100} , ○ : R_H and ▲: S. The total surfactant concentration is 70 wt.%.
- Figure 5 : Lamellar liquid crystal phase : Evolution of the SAXS patterns of the lamellar phase with the Kolliphor (KEL) content in the surfactants mixture (A) and structural parameters of L_α as a function of x_{KEL} (B) and α (C); ■ : d_{001} , ★ : d_B , ○ : d_A and ▲: S. The total surfactant concentration is 85 wt.%.

- Figure 6 : Porous materials : Variation of the SAXS patterns as a function of the fine emulsion/P123 micellar solution weight proportion (Em/P123). This proportion is given on the right.
- Figure 7 : Porous materials : TEM images at two magnifications of materials obtained at various fine emulsion/P123 micellar solution weight proportion (Em/P123). This proportion is given above in the middle.
- Figure 8 : Porous materials : Nitrogen adsorption-desorption isotherms with the corresponding pore size distribution (insert) as a function of the fine emulsion/P123 micellar solution weight proportion. (Em/P123). This value is given in the bottom left.
- Figure 9 : Porous materials : Variation of the specific surface area and of the pore volume as a function of the proportion (%) of Em in the starting solution used to prepare the silica materials; ■ : specific surface area ○ : pore volume.
- Figure 10 : Porous materials : SEM images of the samples prepared with different Em/P123 weight proportions. This value is given on the right.
- Figure 11 : Porous materials : Variation of the weight percentage of released methanol as a function of the proportion (%) of Em in the starting solution used to prepare the silica materials.

Table 1 : Micelles diameter and hydrophobic radius of Kolliphor/P123 mixed micelles. The total concentration of surfactant in water is equal to 5 wt. %.

Sample	Micelles diameter (nm)*	Micelles diameter (nm)**	Hydrophobic radius R_H (nm)
Kolliphor	13.9	14.0	3.5
Kolliphor/P123 = 3	16.6	17.0	4.3
Kolliphor/P123 = 1	17.8	18.0	4.5
Kolliphor/P123 = 0.33	19.6	20.0	4.0
P123	24.3	25.0	3.9

* Values obtained from GIFT analysis

** Values obtained from the excess electron density profiles

Figure 1

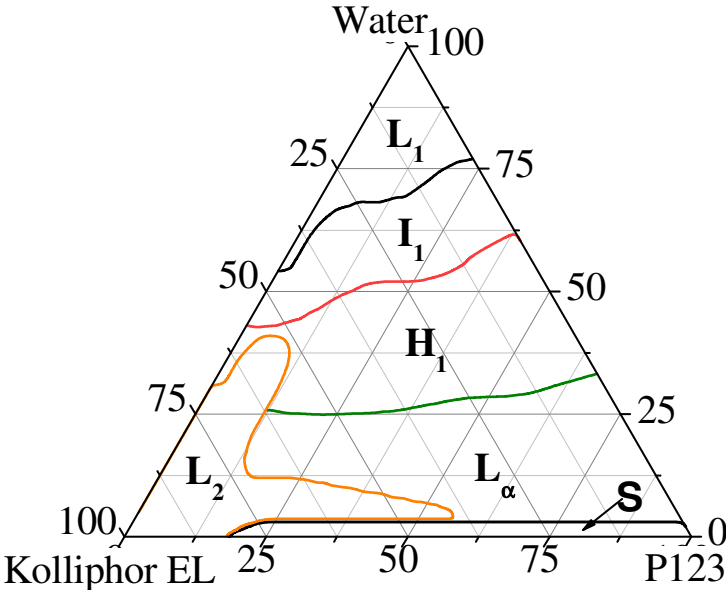


Figure 2

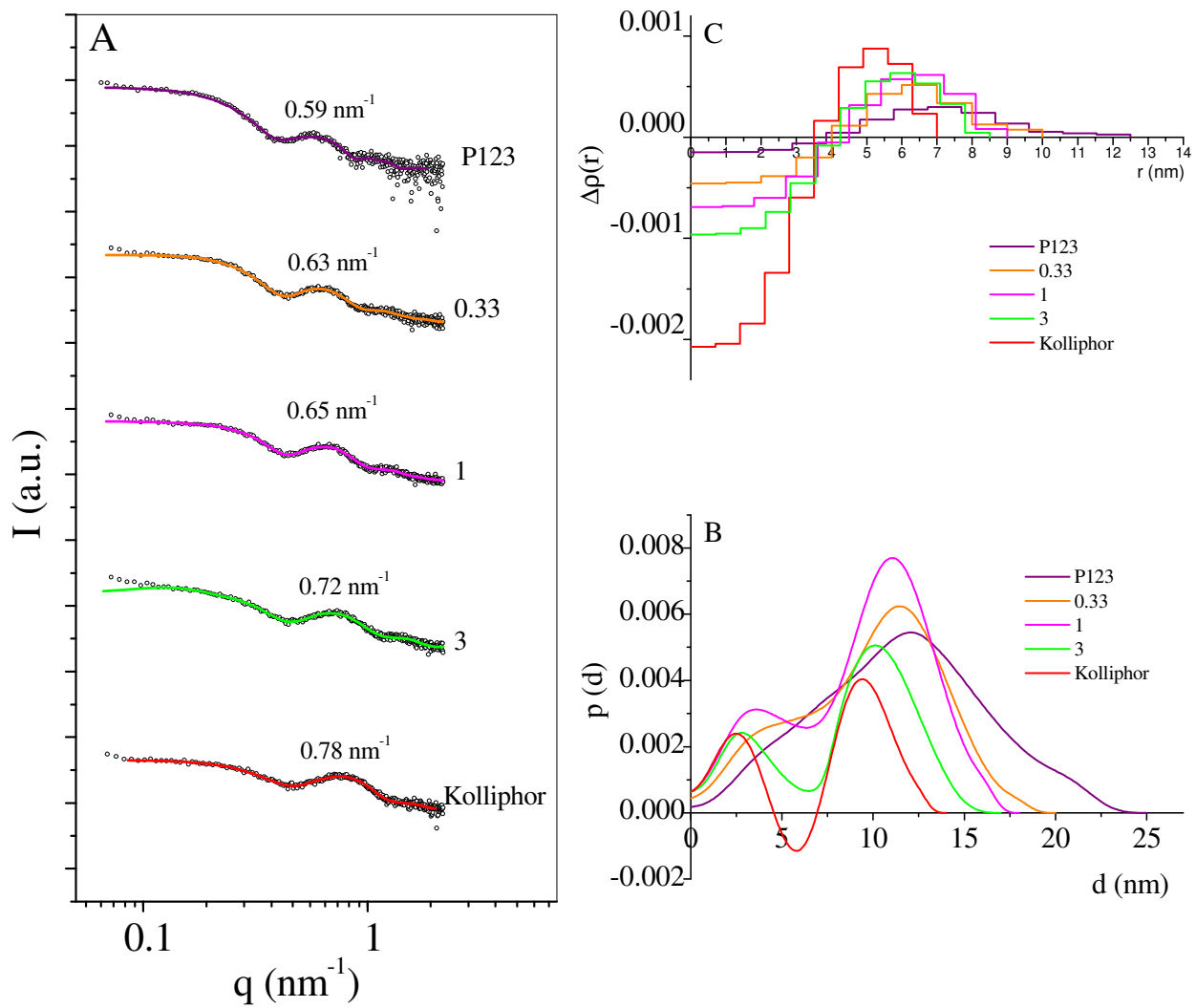


Figure 3

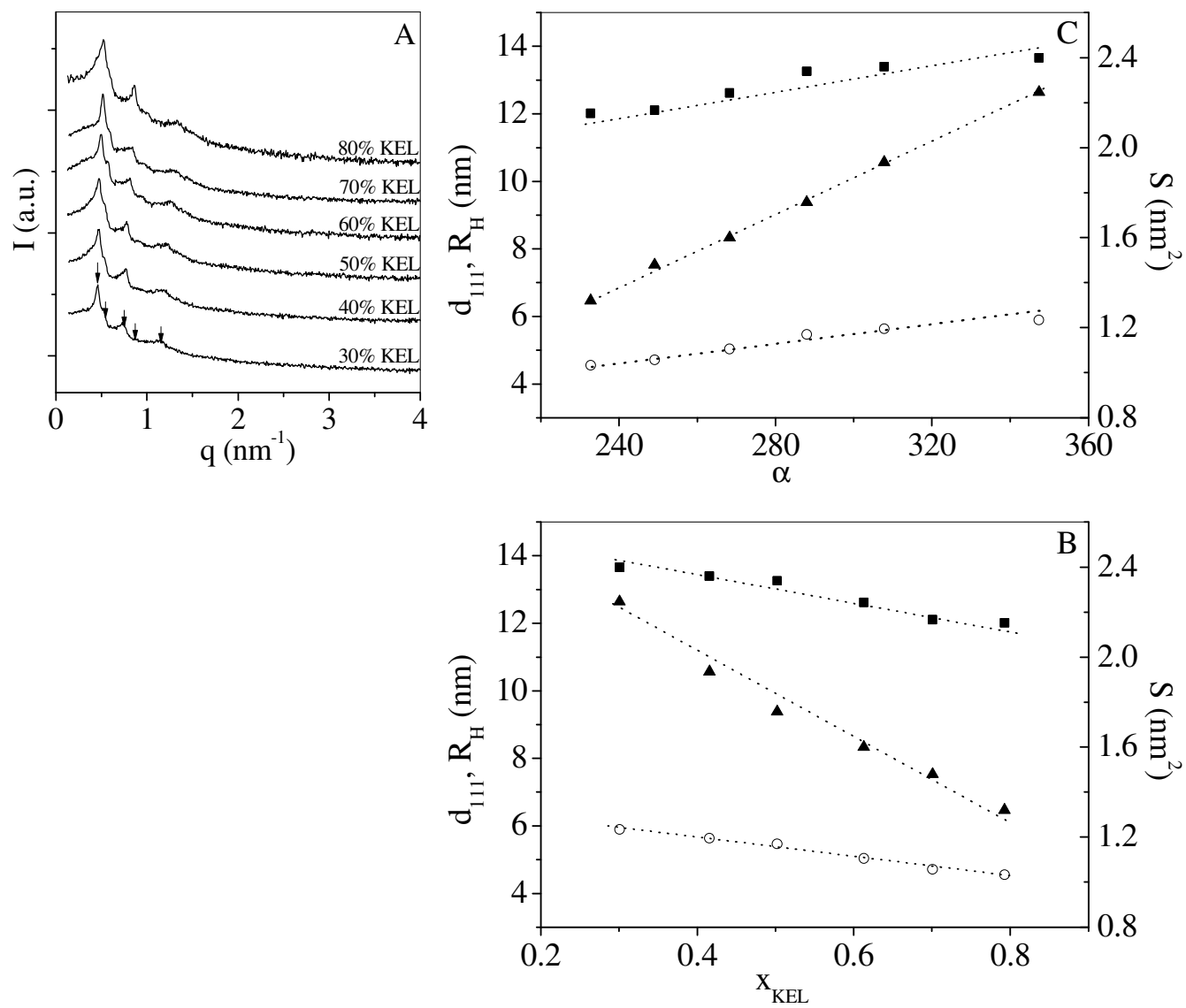


Figure 4

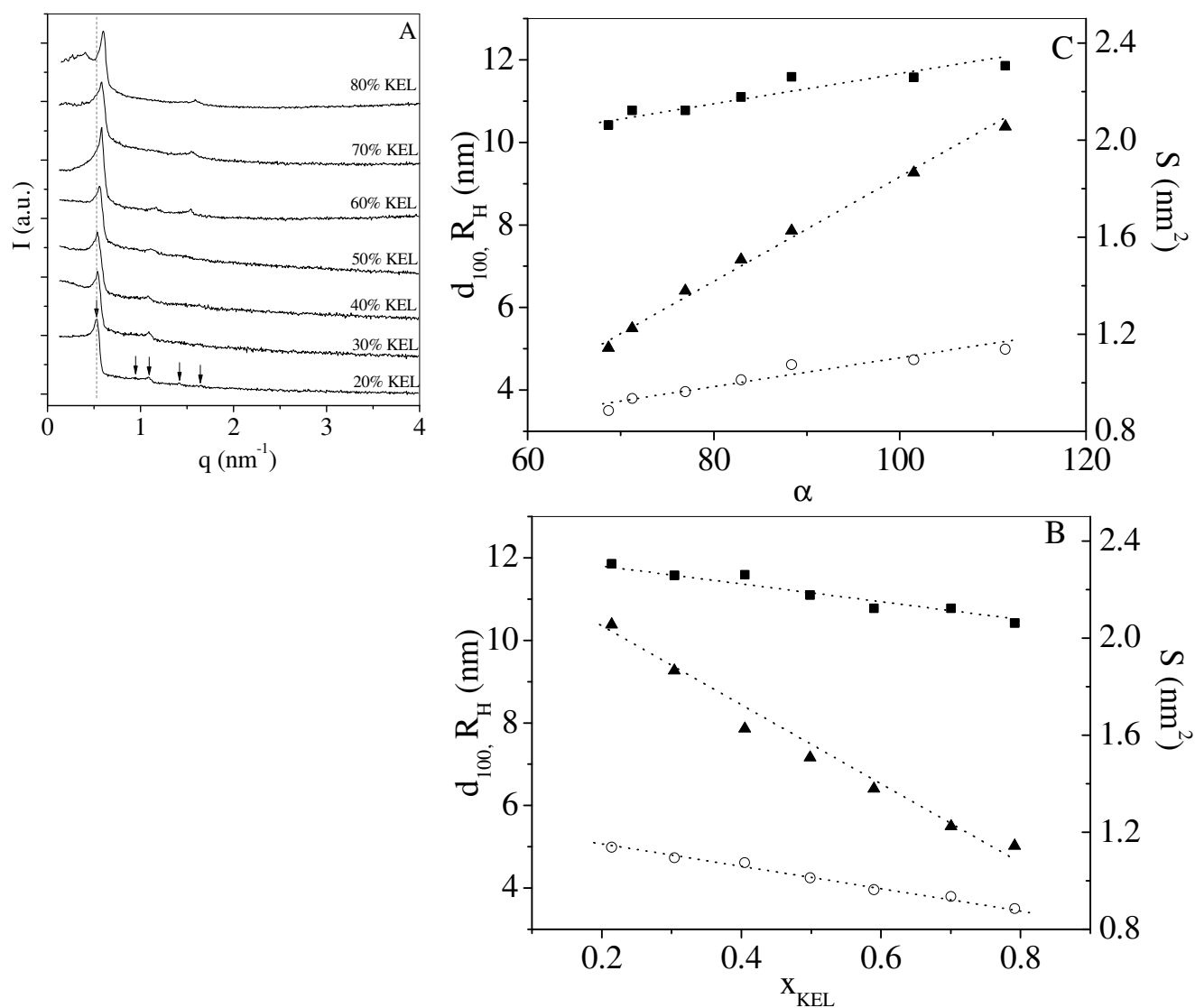


Figure 5

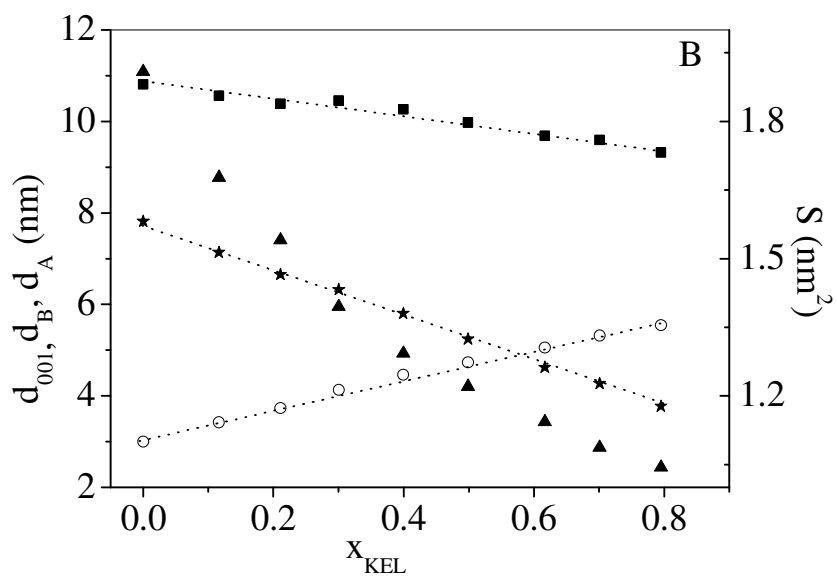
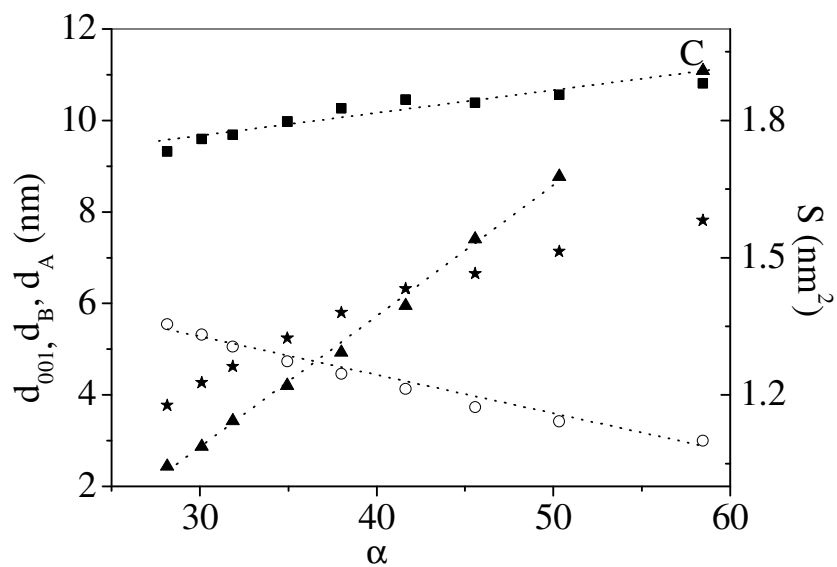
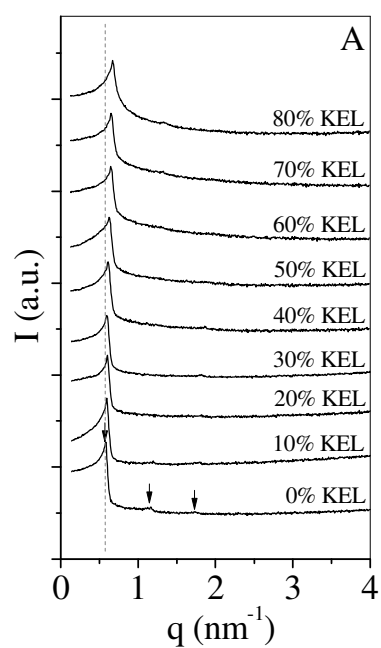


Figure 6

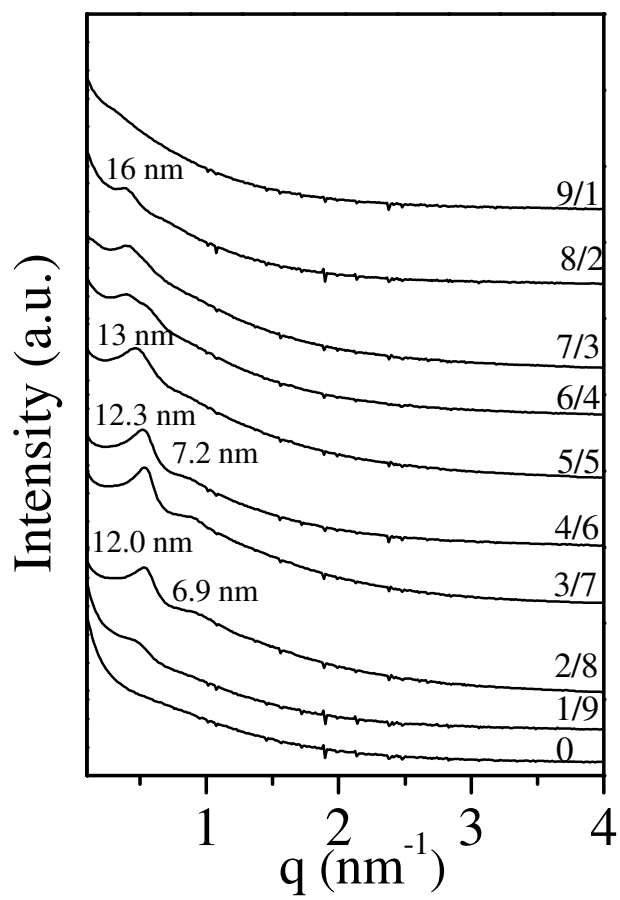


Figure 7

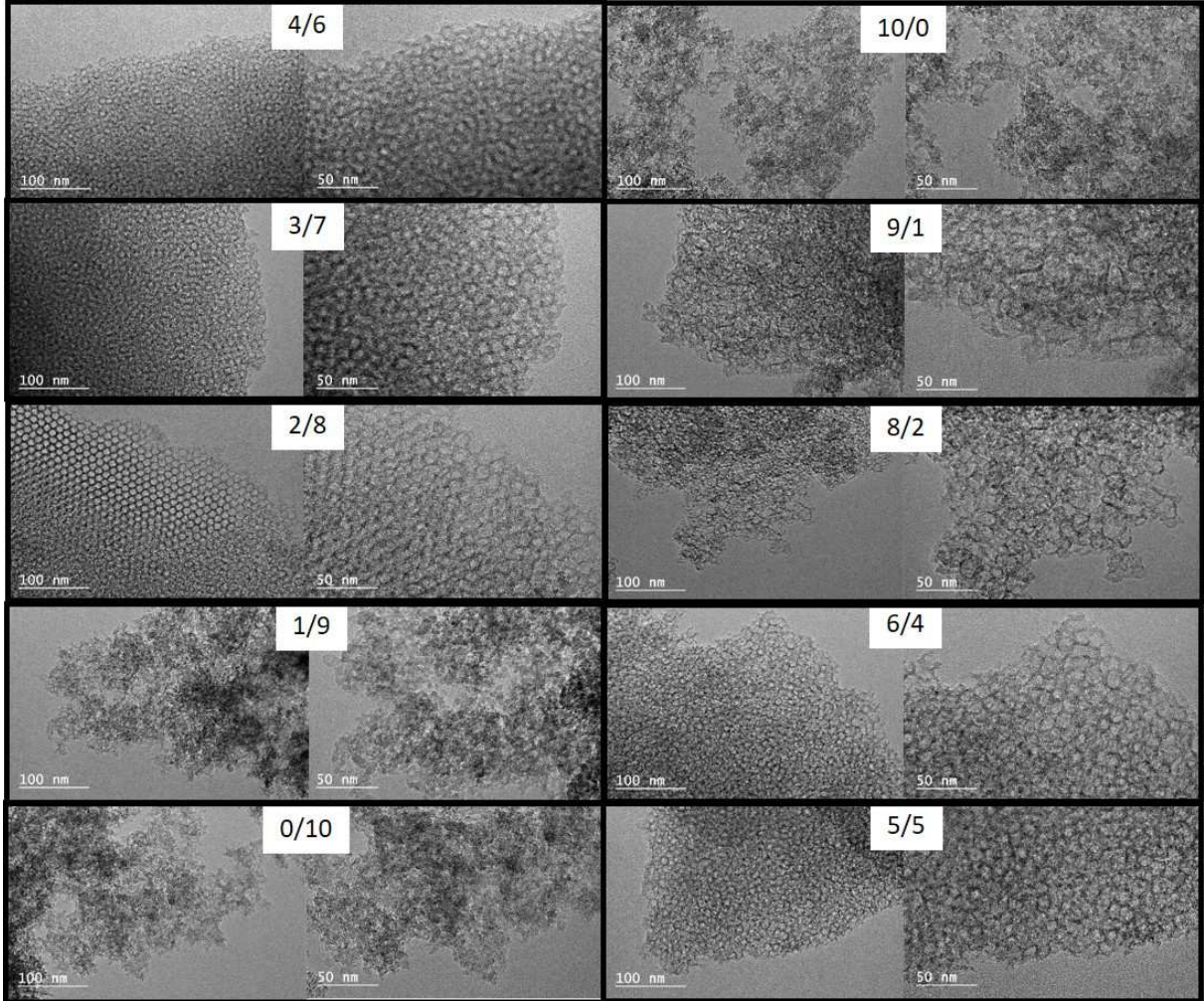


Figure 8

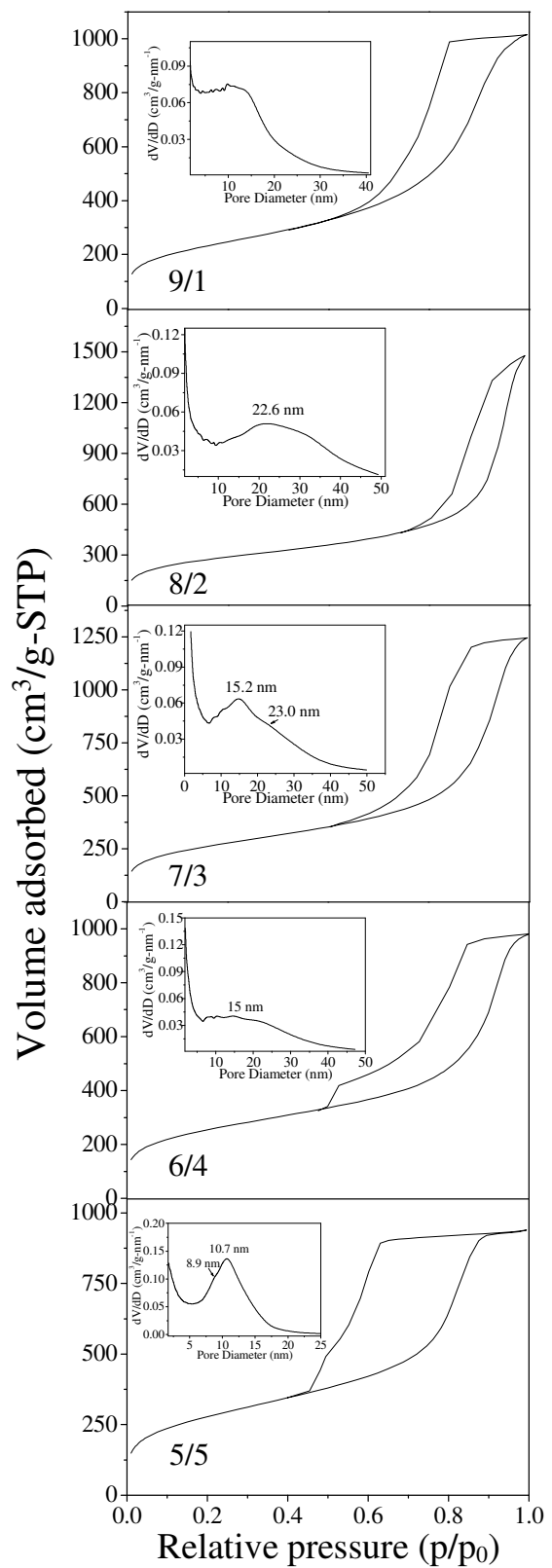
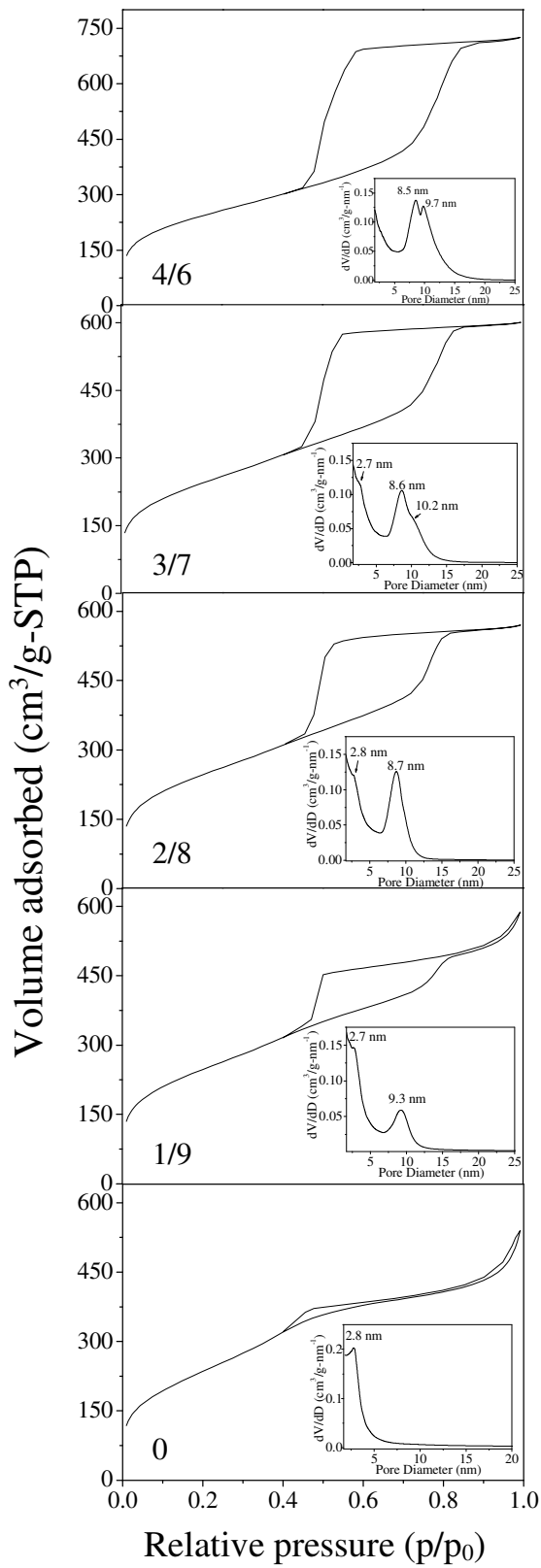


Figure 9

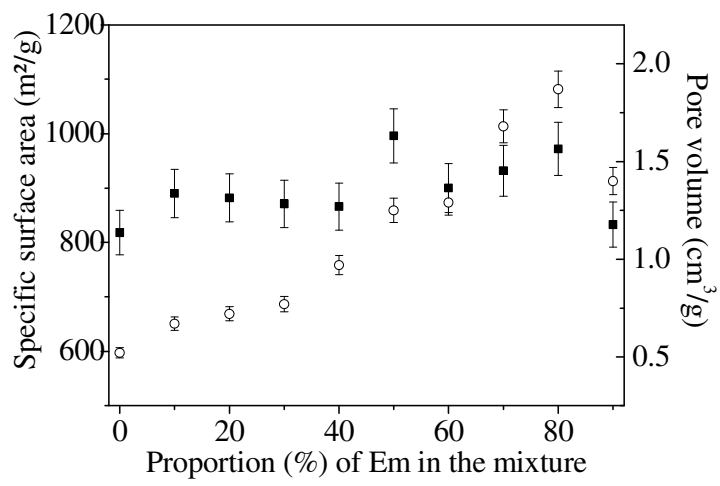


Figure 10

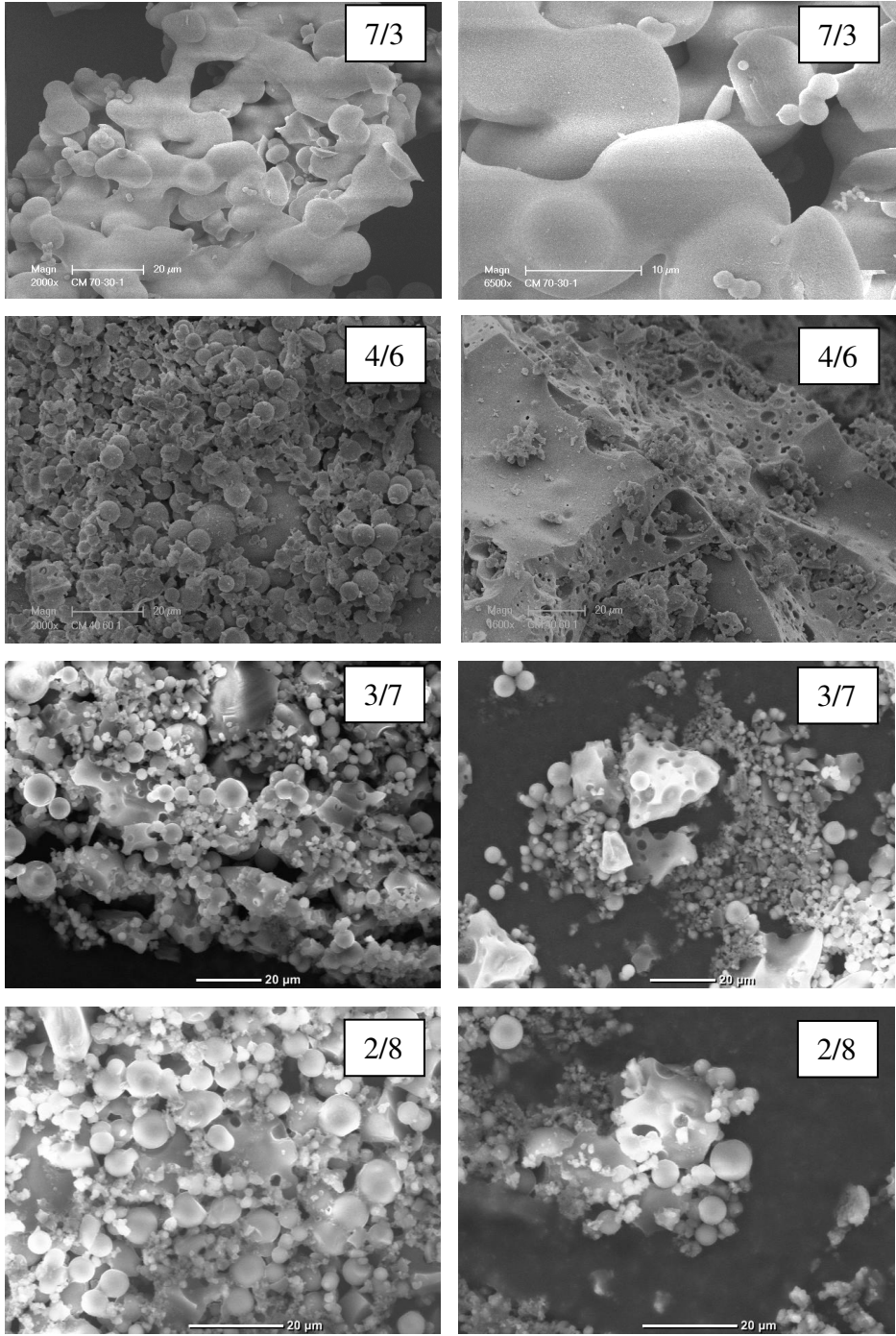


Figure 11

